Positive Role of Fluorine Impurity in Recovered $LiNi_{0.6}Co_{0.2}Mn_{0.2}O_2$ Cathode Materials

Yadong Zheng [a], Ruihan Zhang [a], Panawan Vanaphuti [a], Yangtao Liu [a], Zhenzhen Yang [b], and Yan Wang [a,*]

[a] *Department of Mechanical Engineering, Worcester Polytechnic Institute, Worcester, MA 01609, USA*

[b] *Chemical Sciences and Engineering Division, Argonne National Laboratory, Lemont, IL 60439, USA*

***Correspondence:** yanwang@wpi.edu (Yan Wang), Tel.: +1 508-831-5453

KEYWORDS: *Lithium-ion batteries, Hydrometallurgical recycling, $LiNi_{0.6}Co_{0.2}Mn_{0.2}O_2$ (NCM622) cathode, Fluorine impurity, Electrochemistry*

ABSTRACT

The lithium-ion battery (LIB) recycling is considered as an important component to enable the industry sustainability. A massive number of LIBs in portable electronics, electric vehicles and grid storage will eventually end up in wastes, leading to serious economic and environmental problems. Hence, tremendous effort has been made to improve hydrometallurgical recycling process since it is the most promising option for handling end-of-life LIBs owing to its wide applicability, low cost and high productivity. Despite these advantages, some extra elements (Al, Fe, C, F, etc.) remain as impurities in the removal process and retain in the solution which is a great challenge to obtain high-quality cathode material. In this work, the impacts caused by fluorine impurity on $LiNi_{0.6}Co_{0.2}Mn_{0.2}O_2$ (NCM622) cathode via hydrometallurgical co-precipitation are intensively investigated for the first time. Our results show that up to 1 at% fluorine impurity brings positive influence on the recovered material due to a higher Ni^{2+} ratio on the surface of cathode particles. In addition, the presence of fluoride ion during co-precipitation could lead to the formation of holes in cathode particles which improves rate capability and cyclability dramatically. Compared to virgin, the capacity of NCM622 material with 0.2 at% fluorine impurity is boosted by ~8% (167.7 mAh/g) with a remarkable capacity retention of 98.0% after 100 cycles at 0.33C. Besides, cathode with 0.2 at% fluorine impurity shows a far better rate performance, especially at high rates (~7% increased at 5C), than that of virgin. These results convince that low concentration of fluorine impurity is desirable in hydrometallurgical

recycling process. More importantly, this study offers implications in the design of high performance NCM622 cathode materials via co-precipitation production with ion doping in the near future.

1. Introduction

Rapid expansion in the global market of lithium-ion batteries (LIBs) from portable devices to electric vehicles is imperative, to bring convenience to consumers, to meet targets for reducing carbon emission and to modernize our daily life. Since LIBs were firstly commercialized by Sony in 1991, they have gradually shown dominance in a variety of energy storage applications because of their high energy, light weight, long cycle-life and other advantages.[1,2] In 2019, sales of electric vehicles (EVs) exceeded two million cars worldwide. The fast-growing EV markets, which expanded by an annual average of 60% between 2014 and 2019, reached the stock of 7.2 million in 2019. According to conservative estimates, the stock volume would grow to above 30 million by the end of this decade.[3,4] Besides, mainstream cathode materials used in LIBs (NCM for example) consist of heavy metals such as nickel and cobalt which are not only toxic but also expensive and limited. Undoubtably, the cumulative burden of battery waste in the coming decades will pose a big threat to environment as well as sustainable economy unless there is an ultimate solution to manage end-of-life LIBs. Motivated by this fact, researchers have been working on developing favorable LIB-recycling technologies for years. To date, the reported recycling technologies mainly include three categories as follows: pyrometallurgical recycling, hydrometallurgical recycling, and direct physical recycling. Hydrometallurgical process, due to its high recovery efficiency, large-scale production capability as well as low energy cost, has been widely adopted both in research and industry as a promising approach for battery recycling.[5-8]

A high-efficiency closed-loop hydrometallurgical recycling method was developed by our group for recycling end-of-life LIBs.[5,7,9-11] In this process, spent LIBs were dismantled, crushed, and sieved. Then, the mixed powder went through leaching and subsequent purification process. Afterward, the purified solution was adjusted to the desired concentration ratio to be ready for the following co-precipitation to produce precursors. Final recovered cathode material was obtained by high-temperature sintering of the precursors. This novel recycling method has a high recovery efficiency (~90%) and it is applicable to a wide range of cathode materials ($LiNi_xCo_yMn_zO_2$,

x+y+z = 1). Above all, the recovered cathode products possess a similar or even better electrochemical properties compared to the commercial counterparts. However, the impurity concern, caused by incomplete purification, is a potential issue for the hydrometallurgical technique. In fact, it is difficult to separate all impurity elements such as Al, Fe and Cu from useful transition metals in the solution due to their similar properties. In addition, to remove every single undesired impurity during the purification process is not technically and economically feasible especially in industrial scale aspect.[6,7,12-14] Until recently, study of the impacts on the recovered cathodes as a result of impurities has drawn greater attention among researchers. For example, metal ions such as Al^{3+},[15] Fe^{3+},[16] and Cu^{2+},[17,18] are demonstrated to have positive influences on the final recovered cathodes only if the impurity level is very low. In particular, these cations could replace transition metal ions within cathode crystal by forming precipitates during synthesis. Based on reports, a better ordered structure or slightly expanded lattice that triggered by tiny ion substitution leads to the enhancement of rate capability and capacity retention, whereas excess impurity ions would interfere the structural arrangement, resulting in a bad cathode morphology as well as the formation of impurity phase which causes significant deterioration in cathode electrochemical performance.[15,18] Carbon, a common insoluble impurity coming from conductive additives, is proved to be an adverse factor in hydrometallurgical recycling. Although carbon impurity does not participate in co-precipitation, cathode particles will show a much higher surface Co^{2+} concentration under the presence of carbon after sintering which contributes to the worse cation mixing and poor average capacity.[19] Beyond those impurities mentioned above, another critical concern is the anion impurity, for example fluorine released by $LiPF_6$ lithium salt,[20-22] but little effort has been made to investigate the impacts on synthesized products via hydrometallurgical recycling due to the existence of F^- in the solution. Hence, designing a series of trial reactions with different amount of fluorine impurity to monitor the change in the recovered precursors and cathodes is essential to achieve a better understanding of impurity control in hydrometallurgical recycling.

In this study, a comprehensive investigation on the performance of recovered NCM622 materials under the influence of fluorine impurity via hydrometallurgical synthesis is firstly conducted. Extra fluorine source NaF with the content of 0.2 at%, 1 at% to 5 at% (relative atomic percent of the total transition metals, Ni+Co+Mn = 1) is added in metal sulfate solution prior to co-precipitation reaction as an impurity involved

in recycling process. The NCM622 virgin material (denoted as VNCM) and fluorine impurity affected materials (denoted as 0.2FNCM, 1FNCM and 5FNCM) are examined and studied. It is revealed that fluoride ions during co-precipitation lead to the creation of holes inside precursor particles. After sintering, fluoride ions are found to occupy oxygen sites in cathode crystal and mainly form bonds with Ni ions (NiF_2) which notably increases the ratio of Ni^{2+}/Ni^{3+} on the particle surface. Also, bulk diffusivity gets better owing to a minor lattice expansion and a well-ordered structure when fluorine impurity level is not too high. Both 0.2FNCM and 1FNCM samples display an excellent discharge capacity of ~167 mAh/g (~8% better than VNCM) with a superb capacity retention of ~98% (VNCM 94.8%) after 100 cycles at 0.33C. Moreover, compared to virgin, all FNCM cathodes possess a superior rate capability, especially at high rates. Indeed, holes in cathode particles, high surface Ni^{2+} content and improved bulk lithium diffusivity surely demonstrate the positive role of fluorine impurity in hydrometallurgical recycling. However, the cobalt oxidation state on cathode surface would be affected if too much fluoride is introduced in NCM622 crystal lattice. A high Co^{2+} concentration is detected on 5FNCM cathode surface, resulting in a poor cation ordering and structure stability which makes it the worst among all F-doped NCM622 in terms of electrochemical properties. The results indicate that fluorine impurity has a very positive effect in battery hydrometallurgical recycling and a very high level of fluoride ion content (> 1 at%) should be prevented during the process. Furthermore, our study proves the feasibility of mass production of "boosted" NCM622 cathodes by hydrometallurgical approach with the help of fluoride additives.

2. Experimental section

2.1. Material synthesis

Cathode materials were synthesized by co-precipitation reaction and post-sintering process, in which transition metal ions M^{2+} (M = Ni, Co, Mn) coprecipitate to form $Ni_{0.6}Co_{0.2}Mn_{0.2}(OH)_2$ precursor in alkaline solution then a mixture of dried precursors and lithium salt was sintered to obtain $LiNi_{0.6}Co_{0.2}Mn_{0.2}O_2$ (NCM622) as the final cathode samples.[10,23]

Metal sulfate hydrates $NiSO_4 \cdot 6H_2O$, $CoSO_4 \cdot 7H_2O$ and $MnSO_4 \cdot H_2O$ were added into deionized (DI) water at a stoichiometric ratio of 6:2:2 to obtain 2 M metal sulfate solution. For impurity-involved sample preparation, NaF salt was mixed into the metal sulfate solution with different concentrations (0.2 at%, 1 at% and 5 at%). Prior to the

start, 0.5 M $NH_3 \cdot H_2O$ was filled into a 5 L continuous stirred-tank reactor (CSTR) as a complexing agent. Then, the metal sulfate solution and ammonia solution were pumped into the reactor with a controlled flow rate. Meanwhile, 7.5 M NaOH solution was added into the reactor by a peristaltic pump to keep the reaction at a desired pH condition. The co-precipitation reaction was operated continuously for 12 hrs at a steady condition of pH = 11 and T = 55℃ under nitrogen protection. After reaction, synthesized precursors were filtered and washed with DI water to remove residuals until pH reduced to 7, then precursor powders were dried in oven at 130 ℃ overnight. To obtain cathode materials, precursors were mixed with Li_2CO_3 in a mortar at a stoichiometric ratio of 1:1.05 (5% excess of lithium salt was used in order to compensate for the loss of lithium ions during sintering). Next, the mixture underwent a two-step sintering process: (I) heated up to 450 ℃ for 5 h then cooled down to room temperature, (II) heated up to 850 ℃ for 18 h then followed by a same cooling method (ramp rate was fixed to 2 ℃ per minute).[15,18,19] In the end, a total number of four cathode materials were obtained: $LiNi_{0.6}Co_{0.2}Mn_{0.2}O_2$ (VNCM), and $LiNi_{0.6}Co_{0.2}Mn_{0.2}F_xO_{2-x}$ (x = 0.002, 0.01 and 0.05, named as 0.2FNCM, 1FNCM and 5FNCM, respectively).

2.2. Material characterization

The particle morphologies and microstructures were observed by scanning electron microscopy (SEM, JEOL JSM-7000F) coupled with energy-dispersive spectroscopy (EDS) to analyze element composition. Inductive coupled plasma mass spectroscopy (ICP-MS) was utilized to measure the precise concentrations of all metallic elements in the cathodes. The phases of each sample were identified by powder X-ray diffraction (XRD, PANalytical Empyrean) with Cu Kα (λ = 1.54 Å) and a step size of 0.02° per scan. To acquire lattice parameters, the following Rietveld refinement was conducted via FullProf software and the powder structure of $LiNi_{0.6}Co_{0.2}Mn_{0.2}O_2$ (PDF# 00-066-0854) was chosen as the reference model. X-ray photoelectron spectroscopy (XPS) data for all cathodes was acquired using PHI 5000 VersaProbe II system (Physical Electronics) to investigate element composition and the oxidation state of transition metals. The X-ray source was operating at 25 W equipped with monochromatic Al Kα ($h\upsilon$ = 1486.6 eV) which was set at Ar^+ ion and electron beam sample neutralization, fixed analyzer transmission mode. The XPS spectra were calibrated against C-C at 284.8 eV before subsequent deconvolution simulation (spectra were fitted to multiple Gaussian-Lorentz peaks) which was processed on XPSpeak software.

2.3. Electrochemical measurement

CR-2032 coin cells, which consist of cathode electrode, separator, electrolyte and lithium metal as the anode, were assembled in an argon-gas filled glovebox (H_2O, O_2 < 1 ppm) to study the electrochemical performance. The electrodes were prepared by mixing active materials (cathode powder, 80 wt%), conductive carbon (C65, 10 wt%) and polyvinylidene fluoride binder (PVDF, 10 wt%) in N-methyl-2-pyrrolidone (NMP) solvent to form a slurry. The mixed slurry was then cast on an aluminum foil by a doctor blade (MTI) and dried at 60 ℃ overnight. Round electrodes (Φ = 12 mm) were calendared and punched from dried electrode sheet to get a final thickness ~40 μm with an active mass loading of 3.5~4.0 mg/cm^2. The electrode samples were further dried at 120 ℃ overnight in vacuum oven to remove residual NMP and moisture. A trilayer polypropylene-polyethylene-polypropylene membrane (Φ = 16 mm) and 1 M $LiPF_6$ in ethylene carbonate/ethyl methyl carbonate (EC/EMC, 3:7 in wt%) were used as the separator and electrolyte, respectively. The electrochemical performance was tested on Land battery testing system (LAND, CT2001A) between 3.0V and 4.3V (vs. Li/Li$^+$). Specifically, cells were measured under current density of 0.33C and 5C in cycle test, while the current densities were set from 0.1C up to 5C in rate performance test (1C = 175 mAh/g). Tests of cyclic voltammetry (CV) and electrochemical impedance spectroscopy (EIS) were conducted on an electrochemical analyzer (Bio-Logic SAS, VMP3) using the EC-Lab program. In CV test, scanning potential was set between 3.0V and 4.5V (vs. Li/Li$^+$) at a rate of 0.1 mV/s. In EIS test, cells before and after cycles were measured within the frequency range from 100 kHz to 10 mHz at an amplitude of 10 mV. All electrochemical measurements were carried out under the room condition.

3. Results and discussion

3.1. Structure and composition analysis

To monitor the morphology of hydroxide precursors during the synthesis, sample was collected every 3 hrs then analyzed with SEM. Figure S1 shows the precursor morphology at different times in which the average particle diameter and sphericity increases as the reaction time gets longer. At each specified time, no clear difference is observed between samples from 0.2FNCM to 5FNCM, indicating that the presence of fluoride ions within alkaline environment during co-precipitation does not form extra precipitates to inhibit particle growth as well as to impede particle sphericity. The

particle morphology has a close correlation with its physical properties, powder tap density for instance. In Table S1, the tap density also rises as the reaction goes and all FNCM samples share a similar density level at each time section. It is noted that compared to FNCMs, virgin group has a lower powder tap density at 3 hrs, 6 hrs and 9 hrs which is about 77%, 79% and 89% of the average value of precursors affected by fluorine impurity. However, when the precipitation process reaches to the end at 12 hrs, all samples approach to a same density level (~1.90 g/ml). This phenomenon suggests that fluorine impurity has influenced the co-precipitation process, due to an increased powder tap density that caused by faster nucleation and particle growth at its early stages, while brings no prominent changes in the particle morphology and tap density when the reaction comes to steady state.

Figure 1 shows the SEM images of all synthesized NCM622 samples from precursor (column 1), cathode (column 2) to cross-sectional cathode (column 3). A typical near spherical secondary particle composed of numerous tiny flake-like primary particles is observed in Figure 1a_1-c_1. Primary particles are the most fundamental building blocks of synthesized materials. During the reaction, the growth, attachment and aggregation of primary particles produces the spherical secondary particles.[24] For all cathodes shown in Figure 1a_2-c_2, the shape of primary particles turns from flake to polygon after high-temperature precursor sintering. Both precursors and cathodes have a consistent surface morphology as well as secondary particle dimension (~8 μm) which implies that fluorine impurity has negligible impacts on final cathode morphology. However, the particle interior is completely different. According to cross-sectional images given in Figure 1a_3-c_3, holes are found inside FNCM cathode particles (marked by yellow arrows). Besides, with the increase of impurity concentration from 0.2 at% to 5 at%, the hole formation within cathode particles also rises. It can be inferred that fluorine impurity is a key factor to the formation of holes in cathode particles and this extraordinary feature could promote the electrochemical performances based on recent reports.[25-27]

SEM-EDS mapping results of as-prepared cathodes are given in Figure S2 to show the distribution of elements. Transition metal elements Ni, Co and Mn are distributed homogeneously throughout the particles. The images with purple signals also provide

the evidence of fluorine presents in FNCM cathodes. The precise composition of each

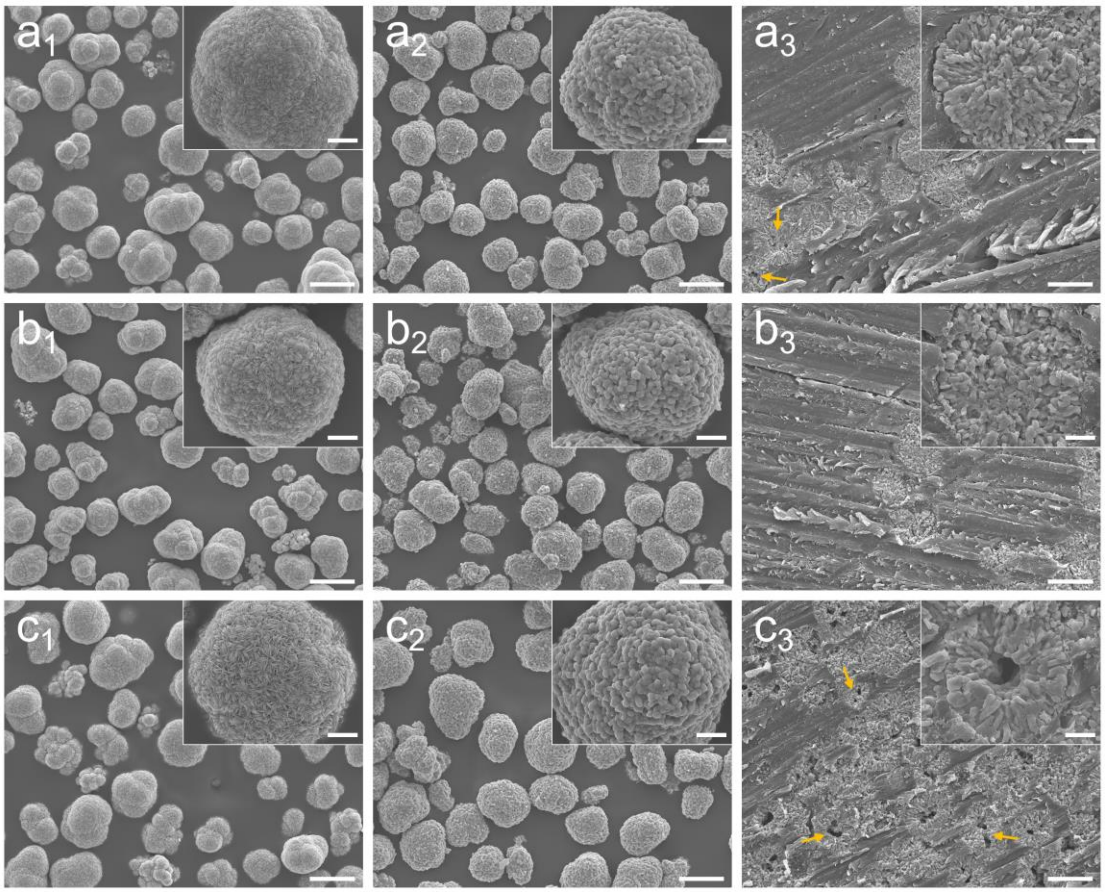

Figure 1. SEM images of 0.2FNCM (a_1-a_3), 1FNCM (b_1-b_3) and 5FNCM (c_1-c_3) with precursors (column 1), cathodes (column 2) and cathode cross-sectionals (column 3) (scale bar 10μm). (Insets: images at higher magnification with scale bar 2μm).

element in NCM622 cathodes at different impurity level was measured by ICP-MS. As shown in Table S2, the atomic ratio of Ni, Co and Mn in all samples keeps close to the theoretical value (6:2:2). Specifically, exact atomic ratio among NCM is calculated to be 6:2.05:2.00, 6:2.11:2.01, 6:2.10:2.00 and 6:2.15:2.05 (Ni = 6) for VNCM, 0.2FNCM, 1FNCM and 5FNCM, respectively. On top of that, the lithium composition remains stable regardless of variation in impurity concentration. Therefore, it can be concluded that fluoride ions do not occupy the sites of cations but to replace oxygens in cathode crystal during the synthesis process.

Further investigation on composition and inner structure of precursor particles was done by cross-sectional SEM-EDS shown in Figure 2. Precursor particles (12 hrs) with holes (marked by yellow arrows) could be confirmed in 5FNCM samples whereas the interior structures of virgin counterparts are completely intact. According to element mapping results in Figure $2a_2$-b_2, the uniform distribution of Ni, Co, Mn and O is also true for synthesized precursors. More importantly, fluorine signal is detected over the

entire cross-section of 5FNCM precursor particles which reveals the participation of F

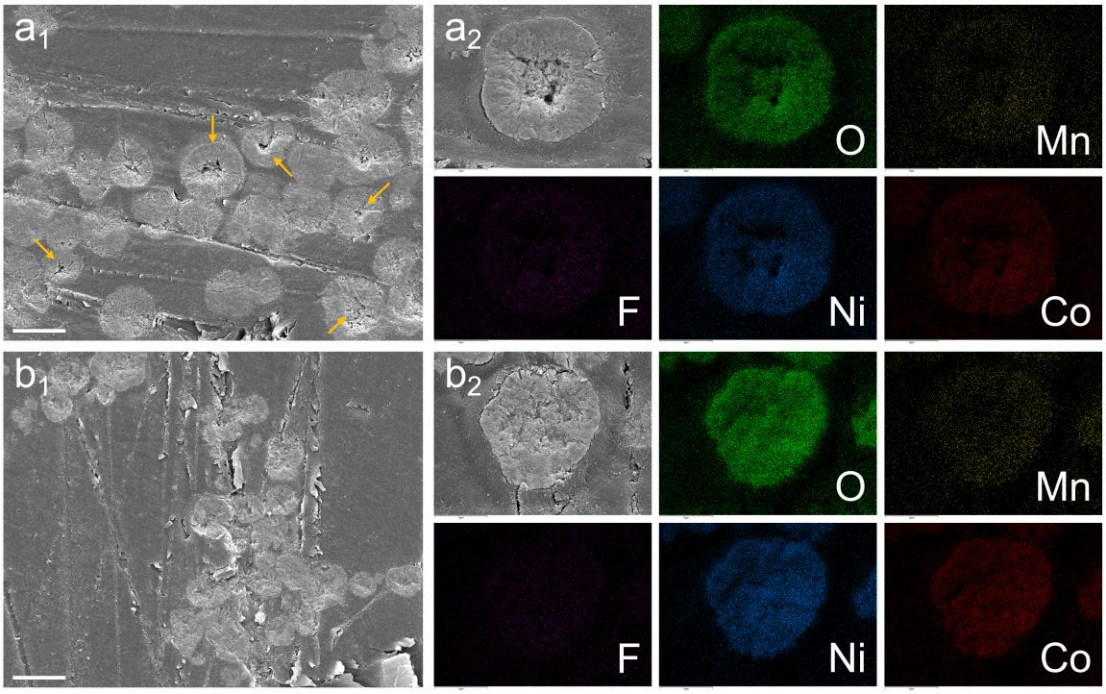

Figure 2. SEM cross-sectional images of precursors for (a_1) 5FNCM and (b_1) VNCM (scale bar 10μm) with corresponding SEM-EDS mapping of each element for (a_2) 5FNCM and (b_2) VNCM.

ions during the co-precipitation process.

The typical mechanism for the synthesis of dense and spherical hydroxide particles via co-precipitation has been mentioned by several groups.[23,24,28] There are two steps to form the precipitates: transition metal ions first coordinate with the ammonia complex agent (1), then slowly precipitate out of the base solution (2). Relevant two-step reactions are as follows:

$$M^{2+} + nNH_3 \rightarrow [M(NH_3)_n]^{2+} \quad (1)$$

$$[M(NH_3)_n]^{2+} + 2OH^- \rightarrow M(OH)_2 \downarrow + nNH_3 \quad (2)$$

At the initial stages, relatively sufficient fluoride ions could lead to the reaction:

$$[M(NH_3)_n]^{2+} + 2F^- \rightarrow MF_2 + nNH_3 \quad (3)$$

which consumes the complex ions $[M(NH_3)_n]^{2+}$ and pushes the equilibrium of the reaction (2) to the left. In this case, the dissolution rate of primary particles exceeds re-crystallization so that holes are created in precursors.[24,29]

Phase and structure of prepared materials are analyzed by powder X-ray diffraction with patterns shown in Figure 3. All patterns in Figure 3a have the same diffraction peaks, corresponded to β-$Ni(OH)_2$ (PDF# 00-059-0462), which is a layered metal hydroxide. There are nine noticeable diffraction peaks in XRD spectra of all cathodes in Figure 3b, perfectly matched $LiNi_{0.6}Co_{0.2}Mn_{0.2}O_2$ (PDF# 00-066-0854), which refers

to a typical layered transition metal oxide. No extra phases or structure changes are

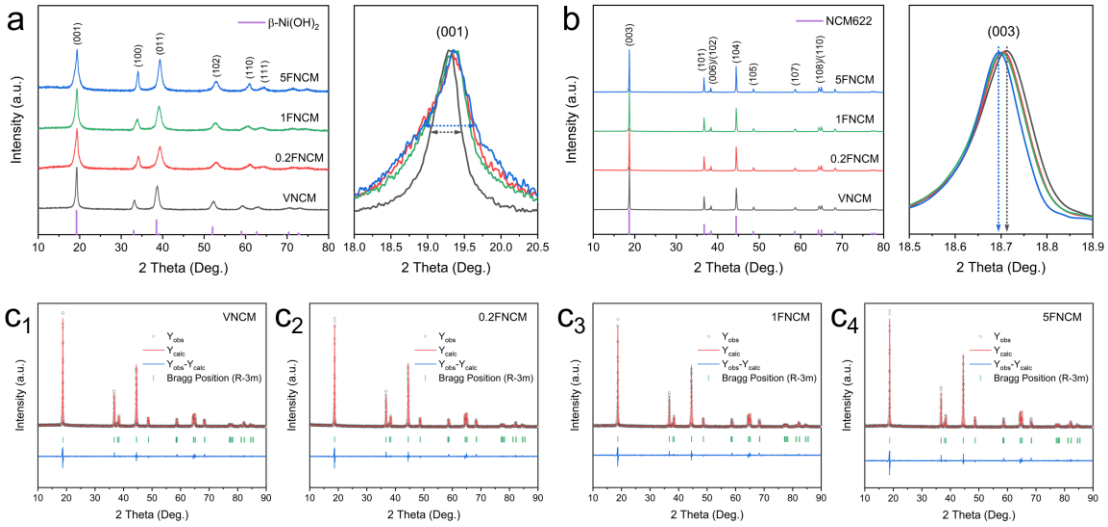

Figure 3. X-ray diffraction patterns of (a) precursors with expansion of (001) plane, (b) cathodes with expansion of (003) plane; (c_1-c_4) Refinement profiles of VNCM, 0.2FNCM, 1FNCM and 5FNCM cathodes.

found in both precursor and cathode patterns. Meanwhile, a pure-phase and well-layered cathode material are maintained. Nonetheless, the (001) peak of FNCM precursors broadens a bit as shown in Figure 3a due to a decrease in primary particle size. Also, (003) plane slightly moves to lower angles for all FNCM cathodes (Figure 3b) as a result of the expansion of c-axis in crystal lattice. It is worth noting that 5FNCM has the lowest $I_{(003)}/I_{(104)}$ ratio (1.59), while other cathodes VNCM (1.81), 0.2FNCM (1.80) and 1FNCM (1.76) hold a much higher value. The higher $I_{(003)}/I_{(104)}$ value indicates a lower Li^+/Ni^{2+} mixing in cathode materials, resulting in a superior electrochemical performance.[30,31] Thus, recovered cathode under the influence of high concentration fluorine impurity (5 at%) is unlikely to be competitive in comparison with the others.

In order to obtain lattice information of recovered cathodes in more detail, Rietveld refinement was used to calculate structure parameters and the rhombohedral crystal

Table 1. Rietveld refinement results of the prepared NCM622 cathodes.

Sample	a-axis (Å)	c-axis (Å)	volume (Å^3)	$O_{Lattice}$	Ni_{Li} (%)	χ^2
VNCM	2.866	14.214	101.07	2.003	3.85	2.77
0.2FNCM	2.866	14.216	101.14	1.992	3.78	2.90
1FNCM	2.866	14.216	101.13	1.983	3.77	2.76
5FNCM	2.867	14.218	101.20	1.934	4.41	3.33

system with space group $R\bar{3}m$ was used as standard. Figure 3c_1-c_4 shows fitted XRD

patterns of all cathode materials and refined crystallographic data are listed in Table 1. As presented in Figure 3c_1-c_4, a satisfactory consistency is achieved between calculated and observed patterns. Plus a relatively small χ^2 is attained for each fitting operation (Table 1), which guarantees all refined results in this work are of high quality.[32] It is clear that the expansion of c-axis is related to the increase of fluorine impurity level, which is consistent with previous studies.[33,34] In fact, the inter-slab distance c of VNCM (14.214Å) is enlarged ~0.03% to 14.218Å for 5FNCM, accompanied with a ~0.13% expansion in cell volume. It should be elucidated that such an expanded lattice will not only reduce the resistance for Li diffusion, but also it could cut down the energy barrier of cation exchange (Li^+/Ni^{2+}) between layers.[35] Apparently, compared to 0.2FNCM and 1FNCM, 5FNCM suffers from the worst cation mixing (4.41%) due to its excess lattice expansion, whereas other cathodes with minor modification in crystal structure remain in good condition. The replacement of O^{2-} with F^- is believed to be the reason to induce appreciable changes to the NCM lattice parameters. It has been reported that the inclusion of fluorine can lead to the reduction of TM ions for charge compensation. Since TM ions with lower oxidation state have a larger radius, when an increasing number of O^{2-} is substituted by F^- under the influence of higher impurity concentration (which is further proved by the decline in $O_{Lattice}$ value), the presence of more bigger TM ions conforms to the greater lattice expansion.[33,34] These results suggest that fluorine impurity (< 1 at%) could enhance Li diffusivity in cathodes via optimized lattice modification, whereas the well-ordered structure would be damaged when too much impurity (> 5 at%) is involved.

3.2. Valence and diffusion analysis

XPS test was employed to investigate materials composition and elements valence states in the as-prepared cathodes. The high-resolution XPS spectra of Ni 2p, Co 2p and Mn 2p were discovered as shown in Figure S3. The binding energy of C 1s (284.8 eV) is used to calibrate all the other spectra to compensate for the charging effect.[36] Two main peaks ($2p_{3/2}$ and $2p_{1/2}$) are found in all spectra because of the spin-orbital splitting. The binding energy of TM elements at about 854 eV (Figure S3a), 780 eV (Figure S3b) and 642 eV (Figure S3c) correlates to Ni^{2+}, Co^{3+} and Mn^{4+} respectively, which is in line with typical TM valences in NCM cathodes. It is worth mentioning that a strong widening of the main peak (~780 eV) and a noticeable satellite peak (~786 eV) in bulk Co 2p spectra indicate a strong presence of Co^{2+} at the center of cathode particles.[37] A

survey scan on Na 1s in Figure 4a shows no signal in all samples. Combining the ICP

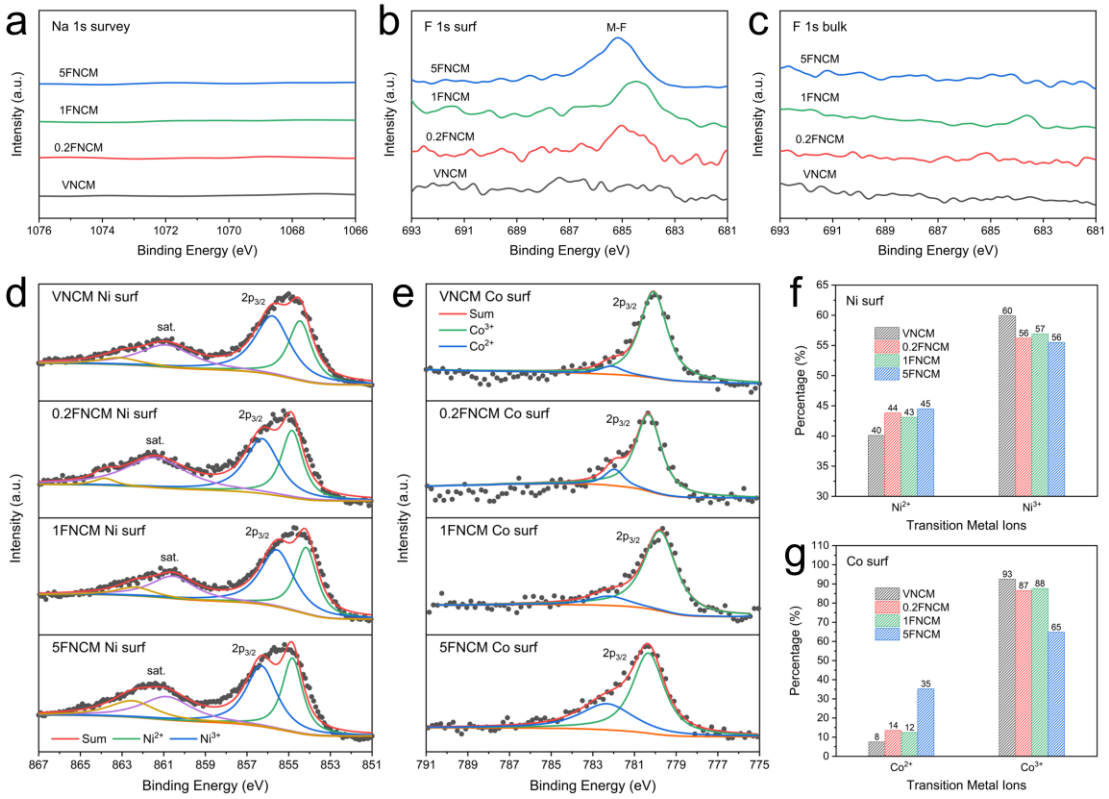

Figure 4. XPS spectra of (a) Na 1s survey scan, (b) F 1s surface and (c) F 1s bulk for cathodes; XPS deconvolution profiles of (d) Ni 2p, (e) Co 2p in surface layer of cathodes; Percentage of (f) Ni^{2+}, Ni^{3+} ions and (g) Co^{2+}, Co^{3+} ions in surface layer of cathodes.

results given in Table S2, this ensures that Na-related substances do not exist in final recovered materials. Figure 4b and Figure 4c display F 1s spectra of surface and bulk for all cathode samples. A strong peak is observed in surface spectra of FNCM cathodes. In Figure 4c, on the contrary, there is no fluorine signal at all. It means that the fluoride ions are mainly clustered at the surface rather than inner part of cathode particles. In addition, the peak (~685 eV) in Figure 4b closely coincides with metal fluorides like LiF and TMF_2 (TM = Ni, Co or Mn).[38,39] Moreover, with the impurity concentration rises from 0.2 at% to 5 at%, the peak intensity increases relatively. Thus, XPS analysis verifies the inclusion of fluoride into cathode materials by the substitution for oxygen, and more importantly, fluoride ions largely reside near the particle surface to form a layer with elevated levels of low valence (+2) TM ions.

To clearly determine the relevant contents of Ni^{2+}/Ni^{3+} and Co^{2+}/Co^{3+} in cathode materials, the spectra deconvolution of $2p_{3/2}$ peak region was performed to calculate the accurate percent ratio of different TM ions. The fitted spectra of Ni $2p_{3/2}$ shown in Figure 4d and Figure S4a indicate a mix of Ni^{2+} and Ni^{3+} in cathodes. Particularly, the Ni $2p_{3/2}$ peak can be split into Ni^{2+} (854.7 eV) and Ni^{3+} (856.5 eV). Similarly, as shown

in Figure 4e and Figure S4b, Co $2p_{3/2}$ peak can be divided into Co^{2+} (782.1 eV) and Co^{3+} (780.2 eV), respectively.[36,40,41] According to Figure 4f, the ratio of Ni^{2+} at particle surface has increased about 4% from 40.1% (VNCM) to an average of 43.8% for all FNCM cathodes. In Figure S4c, as a contrast, the content of Ni^{2+} within the core is only little affected by the additional fluorine impurity, with a largest ratio change less than 1% between VNCM and 5FNCM. This further confirms the fact that more Ni^{2+} ions exist near surface of FNCM cathodes, which could contribute to a higher reversible capacity during cycling. Figure 4g shows only a small amount of Co^{2+} appears in virgin cathode surface. The percentage of surface Co^{2+} increases to ~13% for 0.2FNCM and 1FNCM and reaches as high as 35.2% for 5FNCM. It can be inferred that the reduction of cobalt ions also occurs at the particle surface, especially in the case of a high level of fluoride incorporation (5 at%) into the cathode particle. It should be noted that the large size and charge differences between Li^+ and Co^{3+} ensure a good cation ordering, which is critical for fast lithium-ion diffusion in cathodes.[2] Thus, with a remarkably low surface Co^{3+} concentration, it is not surprising that 5FNCM has a bad cation mixing as revealed previously by XRD analysis. In Figure S4d, similar to nickel, the ratio of Co^{2+} keeps stable (~36%) for all samples at the bulk of the particles.

A series of cyclic voltammetry (CV) tests at various scan rates, Figure S5, were used to determine Li diffusion coefficient (D_{Li}) by using Randles-Sevcik equation:[36,41]

$$I_p^2 = (2.69 \times 10^5)^2 n^3 A^2 D_{Li} C^2 \upsilon \quad (4)$$

where n is the number of electrons transferred in redox reaction (n = 1); A is the electrode surface area (1.13 cm^2 in this work); C is the theoretical molar concentration of Li-ion in NCM crystal (0.05 mol/cm^3) and D_{Li} is the Li diffusion coefficient. The ratio of the squared peak current (I_p^2) to the scan rate (υ) is proportional to the lithium-ion diffusivity (D_{Li}). The linear relationship between these two variables (I_p^2 vs. υ) is depicted in Figure 5a,b where the slope of fitted lines directly reflects the diffusion rate of Li-ion in NCM materials. Then, the slope values are plugged into Randles-Sevcik equation to calculate D_{Li} and the relevant data are given in Table S3 and Figure 5c. The anodic slopes and cathodic slopes shown in Figure 5a,b confirm a strong correlation between anodic and cathodic diffusivity which represent the Li diffusion during de-lithiation and lithiation, respectively. The D_{Li} of VNCM is calculated to be 1.57×10^{-10} cm^2/s (anodic) and 4.24×10^{-11} cm^2/s (cathodic), which are in accordance with recent reports.[42,43] According to the slopes, 0.2FNCM and 1FNCM have a larger value of D_{Li}

compared to the virgin standard, while the Li-ion diffusion condition in 5FNCM is

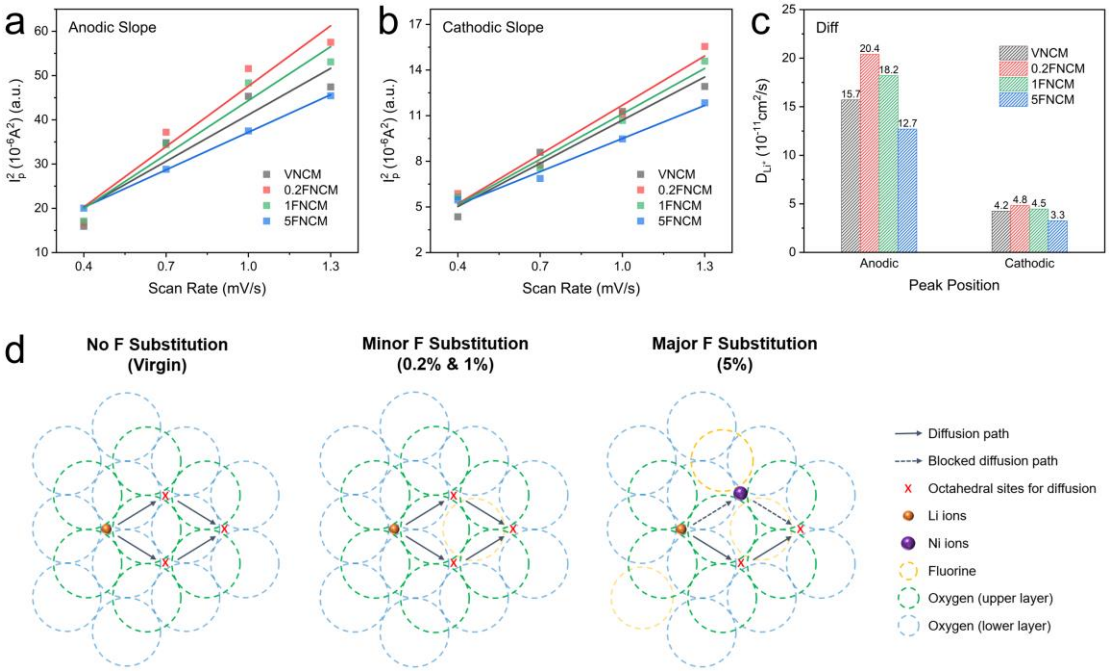

Figure 5. Plot of fitting lines between peak current (I_p^2) vs. scan rate (ν) from CV curves for (a) anodic side and (b) cathodic side; (c) Calculated Li-ion diffusion coefficient, and (d) illustration of Li-ion diffusion within different cathode crystals.

the worst of them all. In particular, 0.2FNCM has the highest Li diffusion coefficient of 2.04×10^{-10} cm^2/s (anodic) and 4.83×10^{-11} cm^2/s (cathodic) which are about 30% and 14% greater than that of virgin standard, indicating that 0.2FNCM could possess the best electrochemical performance among all prepared samples. The lattice images in Figure 5d demonstrate the effects on ionic diffusion caused by different level of fluoride inclusion in NCM crystal. It should be noted that the octahedral sites (marked by red x) between close-packed oxygen ions are essential for Li-ion diffusion within layers. When minor fluoride substitution occurs (< 1 at%), the diffusion paths will still remain feasible. Since fluoride ions have a smaller ionic radius (~1.3 Å) and charge number compared to oxygen ions (~1.4 Å), such a substitution could result in an enlarged interspace and a reduced energy barrier that is responsible for the increase of Li-ion diffusivity.[44] However, excessive fluoride inclusion (> 5 at%) will trigger a considerable deterioration in cation ordering. Therefore, more diffusion routes will be blocked by the mismatched Ni^{2+} ions which leads to a bad diffusion efficiency.

3.3. Mechanisms and electrochemical performance

Figure 6 is a schematic diagram to illustrate the positive influences on the recovered NCM622 cathodes that are caused by fluorine impurity. By intervening the reaction

equilibrium during co-precipitation, fluoride ions promote the dissolution of primary

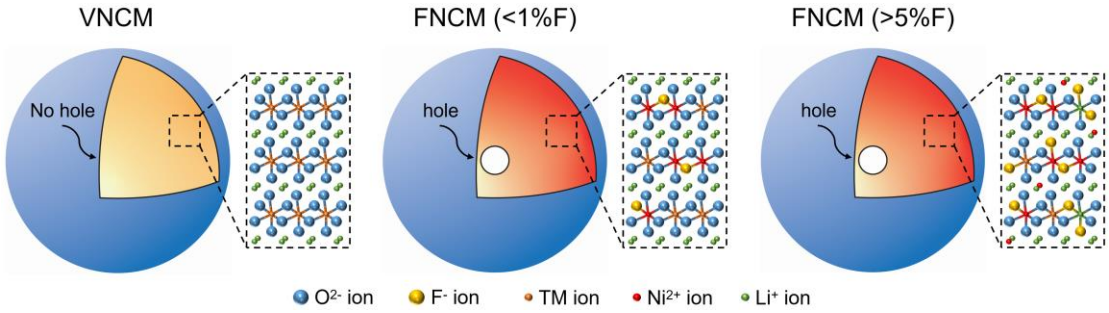

Figure 6. Schematic illustration of the impacts on the NCM622 structure caused by fluorine impurity.

particles and result in the formation of cavity in the precursors. Evidently, after precursors are sintered, cathode particles with a hollow structure could be obtained in all FNCM materials. It is convinced that such a special structure has positive effects on cathode rate performance and cycle stability because the presence of holes reduces the overall Li diffusion distance and could improve particle stability by restraining volume change during cycling.[25,26] Besides, due to charge compensation, a surface layer with an increased ratio of Ni^{2+} is confirmed in all FNCM cathodes, which substantially increases the reversible capacity of materials. Some recent reports also suggest that reducing the amount of high valence Ni^{3+} at near surface is the key to maintain the surface stability.[45-47] In addition, the Li diffusion coefficient will be improved in the FNCM cathodes (< 1 at%) where a tiny portion of lattice oxygens are replaced by fluoride ions which results in a better structure and energy level for ion transport in the lithium layer. Despite all those positive roles, an undesired high level of cation disorder is found in 5FNCM cathode, which in turn brings negative impact on Li diffusion. According to the evidence mentioned so far, it can be inferred that low level of fluorine impurity is beneficial on the recovered NCM622 cathodes via hydrometallurgical process.

In order to understand the electrochemical behavior of the prepared materials, the cyclic voltammetry (CV) was recorded at a scan rate of 0.1 mV/s with a voltage range from 3.0 V to 4.5 V. As shown in Figure S6a-d, one pair of redox peaks (Ni^{2+}/Ni^{4+}) with similar pattern is observed in all samples which means the electrochemical reaction during cycling remain unaffected in FNCM materials. At the first cycle, the oxidation peak of 5FNCM has a noticeable shift to higher voltage (> 4 V) whereas the peaks of others stay around 3.9 V, indicating an increased polarization along with irreversible capacity loss that 5FNCM encounters at the formation cycle. The redox peaks of all materials keep steady at about 3.78 V/3.69 V after a couple of cycles. In

particular, the potential difference between anodic and cathodic peaks at the 5th cycle (ΔE), which represents the reversibility of Li-ion transport during cycling, is relatively small (< 0.1 V) for all cathode materials. The results demonstrate that fluorine impurity (< 5 at%) only has a limited impact on cathode electrochemical reversibility during charge/discharge process. To further analyze the effects of fluorine impurity on ionic conduction, electrochemical impedance spectroscopy (EIS) was measured before and after cycles (150 cycles) at a discharged state in the frequency range from 100 kHz to 10 mHz. The Nyquist plots and the corresponding resistances (R_s, R_{ct}) are given in Figure S6e,f and Table S4. Each of the impedance curve has three characteristics: the initial intercept representing the electrolyte resistance (R_s), a semicircle in the high frequency region associated with the charge transfer resistance (R_{ct}) at the electrode/electrolyte interface and a sloping line in the low frequency region corresponded to the Warburg impedance.[48] As presented in Table S4, the R_s values for all samples are similar and remain stable after cycles, suggesting that the electrolyte composition and conductivity are not influenced by the F-doped cathodes. Notably, the charge transfer resistances (R_{ct}) of all FNCM samples are much lower than those of virgin. Specifically, the R_{ct} values decline about 24%/50% from VNCM to 0.2FNCM before/after cycles, which signifies the positive roles of fluorine impurity with improved Li-ion diffusion as well as electrode surface stability. It is worth noting that the growth of R_{ct} along with the increase of impurity level points out the occurrence of minor side effect caused by fluoride substitution. In general, these results confirm the advantages of fluorine impurity on the NMC622 cathode materials.

A series of electrochemical tests were conducted at the potential range of 3.0 V to 4.3 V (vs. Li/Li$^+$) in order to evaluate the differences in electrochemical performance among synthesized cathodes. The cycling performances at current density of 0.33C and 5C (1C = 175 mAh/g) are measured for 100 cycles. As shown in Figure 7a, cathodes with fluorine impurity (< 1 at%) have a discharge capacity of 167.7 mAh/g after 100 cycles, which is about 8% higher than that of virgin. Meanwhile, according to Figure 7e, both 0.2FNCM and 1FNCM exhibit a superior capacity retention (> 97%), in contrast, VNCM only maintains 94% of its original capacity at 0.33C after 100 cycles. Similar situations are also found in 5C cycling tests. In Figure 7b, 0.2FNCM and 1FNCM has a discharge capacity of 129.2 and 121.1 mAh/g, accompanied by a capacity retention of 95% and 90%, respectively. Virgin cathode, in contrast, has a much poorer properties (112.3 mAh/g, 86%) without the positive impacts from fluorine impurity.

The rate capabilities of prepared samples are analyzed from 0.1C to 5C and the detailed

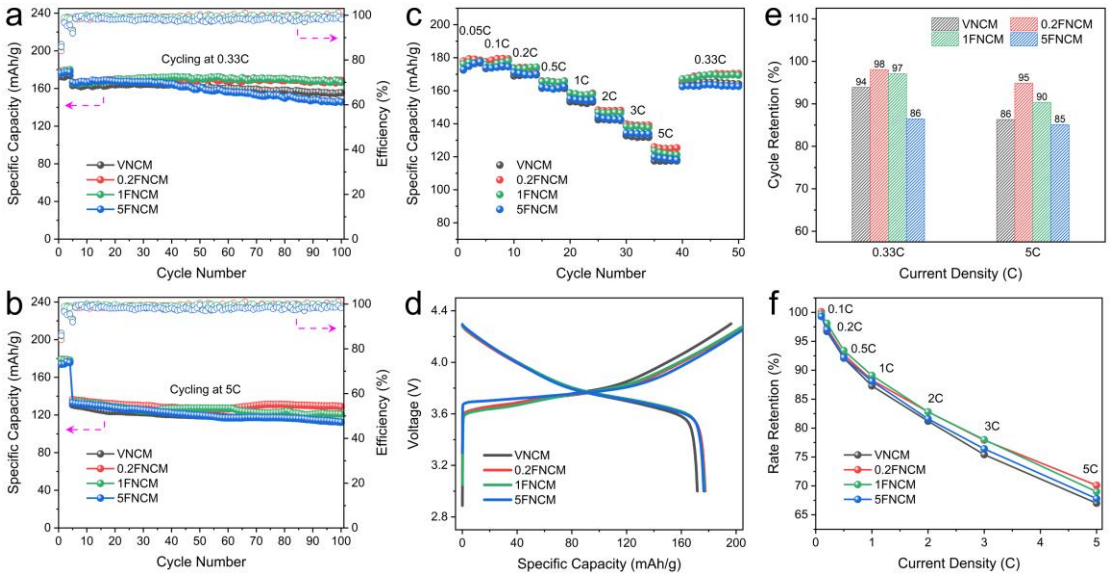

Figure 7. Electrochemical performance of as-prepared samples. (a) cycle at 0.33C, (b) cycle at 5C, (c) rate to 5C, (d) initial charge-discharge profile, (e) retention after 100 cycles, and (f) retention at specific rate relative to formation cycle (0.05C).

values are listed in Table S5. Clearly, all impurity-based cathodes show a better performance in both capacity and retention as shown in Figure 7c,f. In fact, such an improvement over the virgin standard becomes more obvious with the increase of current rate. Therefore, the data from electrochemical tests confirm the positive influence of fluorine impurity which contributes to the outstanding cycle and rate performances of FNCM cathodes. Figure 7d shows the initial charge-discharge profile of different cathodes at 0.05C.VNCM exhibits the lowest capacity of 196.4 and 171.7 mAh/g in the initial charge and discharge process. In the meantime, FNCM cathodes deliver an average capacity of 210 and 177 mAh/g in the formation cycle. Evidently, the boosted initial capacity of FNCM materials is caused by the higher ratio of Ni^{2+} ions in the cathodes which allows more Li^{+} to be activated during cycling. Hence, it can be concluded that the electrochemical property of NCM622 cathode could be significantly improved by fluorine impurity. Moreover, 0.2FNCM and 1FNCM exhibit a far better electrochemical performance than that of VNCM which suggests the potential of using NaF additive to enhance NCM cathode properties via hydrometallurgical synthesis in the future.

4. Conclusion

In this work, a systematic analysis of influences on recovered NCM622 cathodes by fluorine impurity in hydrometallurgical recycling is first reported. It is proved that

fluorine impurity brings lots of positive effects on the synthesized cathode materials. Specifically, the participation of fluoride ions in co-precipitation affects the reaction equilibrium which leads to the creation of holes in hydroxide precipitates. As a result, cathode particles with a hollow structure are obtained after post-sintering, leading to an improved rate capability and cycle stability. Additionally, fluorine impurity has no clear impacts on the morphology, structure, composition and element distribution of the cathode materials. The successful fluoride substitution on oxygen sites in NCM622 near the cathode surface, as proven by XPS, contributes to a higher material capacity and a better cathode surface stability as a result of an increased surface Ni^{2+} content. A minor fluoride inclusion (< 1 at%) in NCM622 lattice is also found to be satisfying since the bulk Li-ion diffusivity is greatly promoted.

The electrochemical characteristics of prepared cathode materials have achieved different levels of improvement due to the positive effects from fluorine impurity. In particular, cathode with 0.2 at% impurity exhibits the best electrochemical performance. 0.2FNCM delivers a reversible capacity of 167.7 mAh/g and a capacity retention of 98.04% after 100 cycles at 0.33C. Besides, the rate capability of FNCM samples is superior to that of VNCM, especially at high current. To sum up, positive roles of fluorine impurity in hydrometallurgical recycling suggest fluoride is not the priority impurity ions which should be completely removed from recovered solution. More importantly, we believe that by adding fluorine additives into reaction, it is feasible to use hydrometallurgical method to produce NCM-based cathodes with enhanced properties in the future.

Associated Content

Supporting Information

The Supporting Information is available free of charge at

Additional figures and tables including SEM of precursors (Figure S1); SEM-EDS mapping of cathodes (Figure S2); XPS spectra of elements in cathodes (Figure S3); XPS deconvolution spectra of Ni and Co in bulk of cathodes (Figure S4); CV curves of electrodes at different scan rates (Figure S5); CV profiles and EIS curves of cathodes (Figure S6); tap density of precursors (Table S1); ICP-MS results of cathodes (Table S2); fitting data in Randles-Sevcik diffusion analysis (Table S3); EIS fitting data (Table S4); and rate performance of all cells (Table S5) (PDF)

Author Information

Corresponding Author

Yan Wang – *Department of Mechanical Engineering, Worcester Polytechnic Institute, Worcester, Massachusetts 01609, United States;*

orcid.org/0000-0003-1060-2956;

Phone: +1 508-831-5453; Email: yanwang@wpi.edu

Authors

Yadong Zheng – *Department of Mechanical Engineering, Worcester Polytechnic Institute, Worcester, Massachusetts 01609, United States;*

orcid.org/0000-0003-4421-9859

Ruihan Zhang – *Department of Mechanical Engineering, Worcester Polytechnic Institute, Worcester, Massachusetts 01609, United States*

Panawan Vanaphuti – *Department of Mechanical Engineering, Worcester Polytechnic Institute, Worcester, Massachusetts 01609, United States;*

orcid.org/0000-0002-8152-1339

Yangtao Liu – *Department of Mechanical Engineering, Worcester Polytechnic Institute, Worcester, Massachusetts 01609, United States*

Zhenzhen Yang – *Chemical Sciences and Engineering Division, Argonne National Laboratory, Lemont, Illinois 60439, United States*

Author Contributions

The manuscript was written through contributions of all authors. All authors have approved the final version of the manuscript.

Notes

The authors declare no competing financial interest.

Acknowledgements

This work was performed through the ReCell Center, which gratefully appreciates the financial support from the U.S. Department of Energy (DOE), Office of Energy Efficiency and Renewable Energy, and the Vehicle Technologies Office. XPS work was conducted at Post Test Facility of Argonne National Laboratory, operated for DOE

Office of Science by UChicago Argonne, LLC, under contract no. DE-AC02-06CH11357.

References

1. Tarascon, J. M.; Armand, M. Issues and Challenges Facing Rechargeable Lithium Batteries. *Nature* **2001,** *414*, 359-367. DOI 10.1038/35104644.

2. Manthiram, A. A Reflection on Lithium-ion Battery Cathode Chemistry. *Nat. Commun.* **2020,** *11*, 1-9. DOI 10.1038/s41467-020-15355-0.

3. International Energy Agency (IEA) Global EV Outlook 2020 (IEA, 2020). https://www.iea.org/reports/global-ev-outlook-2020. (accessed Sept. 8th 2021).

4. Harper, G.; Sommerville, R.; Kendrick, E.; Driscoll, L.; Slater, P.; Stolkin, R.; Walton, A.; Christensen, P.; Heidrich, O.; Lambert, S.; Abbott, A.; Ryder, K. S.; Gaines, L.; Anderson, P. Recycling Lithium-ion Batteries from Electric Vehicles. *Nature* **2019,** *575*, 75-86. DOI 10.1038/s41586-019-1682-5.

5. Zou, H. Y.; Gratz, E.; Apelian, D.; Wang, Y. A Novel Method to Recycle Mixed Cathode Materials for Lithium Ion Batteries. *Green Chem.* **2013,** *15*, 1183-1191. DOI 10.1039/c3gc40182k.

6. Chen, M. Y.; Ma, X. T.; Chen, B.; Arsenault, R.; Karlson, P.; Simon, N.; Wang, Y. Recycling End-of-Life Electric Vehicle Lithium-Ion Batteries. *Joule* **2019,** *3*, 2622-2646. DOI 10.1016/j.joule.2019.09.014.

7. Chen, M. Y.; Zheng, Z. F.; Wang, Q.; Zhang, Y. B.; Ma, X. T.; Shen, C.; Xu, D. P.; Liu, J.; Liu, Y. T.; Gionet, P.; O'Connor, I.; Pinnell, L.; Wang, J.; Gratz, E.; Arsenault, R.; Wang, Y. Closed Loop Recycling of Electric Vehicle Batteries to Enable Ultrahigh Quality Cathode Powder. *Sci. Rep.* **2019,** *9*, 1-9. DOI 10.1038/s41598-018-38238-3.

8. Ciez, R. E.; Whitacre, J. F. Examining Different Recycling Processes for Lithium-ion Batteries. *Nat. Sustain.* **2019,** *2*, 148-156. DOI 10.1038/s41893-019-0222-5.

9. Gratz, E.; Sa, Q. N.; Apelian, D.; Wang, Y. A Closed Loop Process for Recycling Spent Lithium Ion Batteries. *J. Power Sources* **2014,** *262*, 255-262. DOI 10.1016/j.jpowsour.2014.03.126.

10. Sa, Q.; Gratz, E.; He, M. N.; Lu, W. Q.; Apelian, D.; Wang, Y. Synthesis of High Performance $LiNi_{1/3}Mn_{1/3}Co_{1/3}O_2$ from Lithium Ion Battery Recovery Stream. *J. Power Sources* **2015,** *282*, 140-145. DOI 10.1016/j.jpowsour.2015.02.046.

11. Zheng, Z. F.; Chen, M. Y.; Wang, Q.; Zhang, Y. B.; Ma, X. T.; Shen, C.; Xu, D. P.; Liu, J.; Liu, Y. T.; Gionet, P.; O'Connor, I.; Pinnell, L.; Wang, J.; Gratz, E.; Arsenault, R.; Wang, Y. High Performance Cathode Recovery from Different Electric Vehicle Recycling Streams. *ACS Sustain. Chem. Eng.* **2018,** *6*, 13977-13982. DOI 10.1021/acssuschemeng.8b02405.

12. Kruger, S.; Hanisch, C.; Kwade, A.; Winter, M.; Nowak, S. Effect of Impurities Caused by a Recycling Process on the Electrochemical Performance of $Li[Ni_{0.33}Co_{0.33}Mn_{0.33}]O_2$. *J. Electroanal. Chem.* **2014,** *726*, 91-96. DOI 10.1016/j.jelechem.2014.05.017.

13. Chen, X. P.; Chen, Y. B.; Zhou, T.; Liu, D. P.; Hu, H.; Fan, S. Y. Hydrometallurgical Recovery of Metal Values from Sulfuric Acid Leaching Liquor of Spent Lithium-ion Batteries. *Waste Manage.* **2015,** *38*, 349-356. DOI 10.1016/j.wasman.2014.12.023.

14. Peng, F. W.; Mu, D. Y.; Li, R. H.; Liu, Y. L.; Ji, Y. P.; Dai, C. S.; Ding, F. Impurity Removal with Highly Selective and Efficient Methods and the Recycling of Transition Metals from Spent Lithium-ion Batteries. *RSC Adv.* **2019,** *9*, 21922-21930. DOI 10.1039/c9ra02331c.

15. Zhang, R. H.; Zheng, Y. D.; Yao, Z. Y.; Vanaphuti, P.; Ma, X. T.; Bong, S.; Chen, M. Y.; Liu, Y. T.; Cheng, F.; Yang, Z. Z.; Wang, Y. Systematic Study of Al Impurity for NCM622 Cathode Materials. *ACS Sustain. Chem. Eng.* **2020,** *8*, 9875-9884. DOI 10.1021/acssuschemeng.0c02965.

16. Park, S.; Kim, D.; Ku, H.; Jo, M.; Kim, S.; Song, J.; Yu, J.; Kwon, K. The Effect of Fe as an Impurity Element for Sustainable Resynthesis of $Li[Ni_{1/3}Co_{1/3}Mn_{1/3}]O_2$ Cathode Material from Spent Lithium-ion Batteries. *Electrochim. Acta* **2019,** *296*, 814-822. DOI 10.1016/j.electacta.2018.11.001.

17. Sa, Q. N.; Heelan, J. A.; Lu, Y.; Apelian, D.; Wang, Y. Copper Impurity Effects on $LiNi_{1/3}Mn_{1/3}Co_{1/3}O_2$ Cathode Material. *ACS Appl. Mater. Inter.* **2015,** *7*, 20585-20590. DOI 10.1021/acsami.5b04426.

18. Zhang, R. H.; Meng, Z. F.; Ma, X. T.; Chen, M. Y.; Chen, B.; Zheng, Y. D.; Yao, Z. Y.; Vanaphuti, P.; Bong, S.; Yang, Z. Z.; Wang, Y. Understanding Fundamental Effects of Cu Impurity in Different Forms for Recovered $LiNi_{0.6}Co_{0.2}Mn_{0.2}O_2$ Cathode Materials. *Nano Energy* **2020,** *78*, 105214. DOI 10.1016/j.nanoen.2020.105214.

19. Zheng, Y. D.; Zhang, R. H.; Vanaphuti, P.; Fu, J. Z.; Yang, Z. Z.; Wang, Y. Unveiling the Influence of Carbon Impurity on Recovered NCM622 Cathode Material. *ACS Sustain. Chem. Eng.* **2021,** *9*, 6087-6096. DOI 10.1021/acssuschemeng.1c01510.

20. Hanisch, C.; Loellhoeffel, T.; Diekmann, J.; Markley, K. J.; Haselrieder, W.; Kwade, A. Recycling of Lithium-ion Batteries: A Novel Method to Separate Coating and Foil of Electrodes. *J. Clean. Prod.* **2015,** *108*, 301-311. DOI 10.1016/j.jclepro.2015.08.026.

21. Lv, W. G.; Wang, Z. H.; Cao, H. B.; Sun, Y.; Zhang, Y.; Sun, Z. A Critical Review and Analysis on the Recycling of Spent Lithium-Ion Batteries. *ACS Sustain. Chem. Eng.* **2018,** *6*, 1504-1521. DOI 10.1021/acssuschemeng.7b03811.

22. Yu, J. D.; Lin, M. S.; Tan, Q. Y.; Li, J. H. High-value Utilization of Graphite Electrodes in Spent Lithium-ion Batteries: From 3D Waste Graphite to 2D Graphene Oxide. *J. Hazard. Mater.* **2021,** *401*, 123715. DOI 10.1016/j.jhazmat.2020.123715.

23. Lee, M. H.; Kang, Y.; Myung, S. T.; Sun, Y. K. Synthetic Optimization of $Li[Ni_{1/3}Co_{1/3}Mn_{1/3}]O_2$ via Co-precipitation. *Electrochim. Acta* **2004,** *50*, 939-948. DOI 10.1016/j.electacta.2004.07.038.

24. Hua, W. B.; Liu, W. Y.; Chen, M. Z.; Indris, S.; Zheng, Z.; Guo, X. D.; Bruns, M.; Wu, T. H.; Chen, Y. X.; Zhong, B. H.; Chou, S. L.; Kang, Y. M.; Ehrenberg, H. Unravelling the Growth Mechanism of Hierarchically Structured $Ni_{1/3}Co_{1/3}Mn_{1/3}(OH)_2$ and Their Application as Precursors for High-power Cathode Materials. *Electrochim. Acta* **2017,** *232*, 123-131. DOI 10.1016/j.electacta.2017.02.105.

25. Ding, Y. L.; Zhao, X. B.; Xie, J.; Cao, G. S.; Zhu, T. J.; Yu, H. M.; Sun, C. Y. Double-shelled Hollow Microspheres of $LiMn_2O_4$ for High-performance Lithium Ion Batteries. *J. Mater. Chem.* **2011,** *21*, 9475-9479. DOI 10.1039/c1jm10924c.

26. Li, J. L.; Cao, C. B.; Xu, X. Y.; Zhu, Y. Q.; Yao, R. M. $LiNi_{1/3}Co_{1/3}Mn_{1/3}O_2$ Hollow Nano-micro Hierarchical Microspheres with Enhanced Performances as Cathodes for Lithium-ion Batteries. *J. Mater. Chem. A* **2013,** *1*, 11848-11852. DOI 10.1039/c3ta12375h.

27. Zhao, X. X.; An, L. W.; Sun, J. C.; Liang, G. C. $LiNi_{0.5}Co_{0.2}Mn_{0.3}O_2$ Hollow Microspheres-synthesis, Characterization and Application as Cathode Materials for Power Lithium Ion Batteries. *J. Electroanal. Chem.* **2018,** *810*, 1-10. DOI 10.1016/j.jelechem.2018.01.006.

28. van Bommel, A.; Dahn, J. R. Analysis of the Growth Mechanism of Coprecipitated Spherical and Dense Nickel, Manganese, and Cobalt-Containing

Hydroxides in the Presence of Aqueous Ammonia. *Chem. Mater.* **2009,** *21*, 1500-1503. DOI 10.1021/cm803144d.

29. Thanh, N. T. K.; Maclean, N.; Mahiddine, S. Mechanisms of Nucleation and Growth of Nanoparticles in Solution. *Chem. Rev.* **2014,** *114*, 7610-7630. DOI 10.1021/cr400544s.

30. Li, J. Y.; Li, W. D.; Wang, S. Y.; Jarvis, K.; Yang, J. H.; Manthiram, A. Facilitating the Operation of Lithium-Ion Cells with High-Nickel Layered Oxide Cathodes with a Small Dose of Aluminum. *Chem. Mater.* **2018,** *30*, 3101-3109. DOI 10.1021/acs.chemmater.8b01077.

31. Li, H.; Zhou, P. F.; Liu, F. M.; Li, H. X.; Cheng, F. Y.; Chen, J. Stabilizing Nickel-rich Layered Oxide Cathodes by Magnesium Doping for Rechargeable Lithium-ion Batteries. *Chem. Sci.* **2019,** *10*, 1374-1379. DOI 10.1039/c8sc03385d.

32. Toby, B. H. R Factors in Rietveld Analysis: How Good is Good Enough? *Powder Diffr.* **2006,** *21*, 67-70. DOI 10.1154/1.2179804.

33. Binder, J. O.; Culver, S. P.; Pinedo, R.; Weber, D. A.; Friedrich, M. S.; Gries, K. I.; Volz, K.; Zeier, W. G.; Janek, J. Investigation of Fluorine and Nitrogen as Anionic Dopants in Nickel-Rich Cathode Materials for Lithium-Ion Batteries. *ACS Appl. Mater. Inter.* **2018,** *10*, 44452-44462. DOI 10.1021/acsami.8b16049.

34. Vanaphuti, P.; Chen, J. J.; Cao, J. Y.; Bigham, K.; Chen, B.; Yang, L. F.; Chen, H. L.; Wang, Y. Enhanced Electrochemical Performance of the Lithium-Manganese Rich Cathode for Li-Ion Batteries with Na and F CoDoping. *ACS Appl. Mater. Inter.* **2019,** *11*, 37842-37849. DOI 10.1021/acsami.9b13838.

35. Kang, K.; Ceder, G. Factors that Affect Li Mobility in Layered Lithium Transition Metal Oxides. *Phys. Rev. B* **2006,** *74*, 094105. DOI 10.1103/PhysRevB.74.094105.

36. Chen, Z.; Wang, J.; Chao, D. L.; Baikie, T.; Bai, L. Y.; Chen, S.; Zhao, Y. L.; Sum, T. C.; Lin, J. Y.; Shen, Z. X. Hierarchical Porous $LiNi_{1/3}Co_{1/3}Mn_{1/3}O_2$ Nano-/Micro Spherical Cathode Material: Minimized Cation Mixing and Improved Li^+ Mobility for Enhanced Electrochemical Performance. *Sci. Rep.* **2016,** *6*, 1-10. DOI 10.1038/srep25771.

37. Daheron, L.; Dedryvere, R.; Martinez, H.; Menetrier, M.; Denage, C.; Delmas, C.; Gonbeau, D. Electron Transfer Mechanisms upon Lithium Deintercalation from $LiCoO_2$ to CoO_2 Investigated by XPS. *Chem. Mater.* **2008,** *20*, 583-590. DOI 10.1021/cm702546s.

38. Fan, X. M.; Hu, G. R.; Zhang, B.; Ou, X.; Zhang, J. F.; Zhao, W. G.; Jia, H. P.; Zou, L. F.; Li, P.; Yang, Y. Crack-free Single-crystalline Ni-rich Layered NCM Cathode Enable Superior Cycling Performance of Lithium-ion Batteries. *Nano Energy* **2020,** *70*, 104450. DOI 10.1016/j.nanoen.2020.104450.

39. Breddemann, U.; Krossing, I. Review on Synthesis, Characterization, and Electrochemical Properties of Fluorinated Nickel-Cobalt-Manganese Cathode Active Materials for Lithium-Ion Batteries. *Chemelectrochem* **2020,** *7*, 1389-1430. DOI 10.1002/celc.202000029.

40. Fu, Z. W.; Hu, J. T.; Hu, W. L.; Yang, S. Y.; Luo, Y. F. Quantitative Analysis of Ni^{2+}/Ni^{3+} in $Li[Ni_xMn_yCo_z]O_2$ Cathode Materials: Non-linear Least-squares Fitting of XPS Spectra. *Appl. Surf. Sci.* **2018,** *441*, 1048-1056. DOI 10.1016/j.apsusc.2018.02.114.

41. Xu, Q.; Li, X. F.; Sari, H. M. K.; Li, W. B.; Liu, W.; Hao, Y. C.; Qin, J.; Cao, B.; Xiao, W.; Xu, Y.; Wei, Y.; Kou, L.; Tian, Z. Y.; Shao, L.; Zhang, C.; Sun, X. L. Surface Engineering of $LiNi_{0.8}Mn_{0.1}Co_{0.1}O_2$ towards Boosting Lithium Storage: Bimetallic Oxides versus Monometallic Oxides. *Nano Energy* **2020,** *77*, 105034. DOI 10.1016/j.nanoen.2020.105034.

42. Yao, L.; Liang, F. Q.; Jin, J.; Chowdari, B. V. R.; Yang, J. H.; Wen, Z. Y. Improved Electrochemical Property of Ni-rich $LiNi_{0.6}Co_{0.2}Mn_{0.2}O_2$ Cathode via In-situ ZrO_2 Coating for High Energy Density Lithium Ion Batteries. *Chem. Eng. J.* **2020,** *389*, 124403. DOI 10.1016/j.cej.2020.124403.

43. Hong, C. Y.; Leng, Q. Y.; Zhu, J. P.; Zheng, S. Y.; He, H. J.; Li, Y. X.; Liu, R.; Wan, J. J.; Yang, Y. Revealing the Correlation between Structural Evolution and Li^+ Diffusion Kinetics of Nickel-rich Cathode Materials in Li-ion Batteries. *J. Mater. Chem. A* **2020,** *8*, 8540-8547. DOI 10.1039/d0ta00555j.

44. Shannon, R. D. Revised Effective Ionic-Radii and Systematic Studies of Interatomic Distances in Halides and Chalcogenides. *Acta Crystallogr. A* **1976,** *32*, 751-767. DOI 10.1107/S0567739476001551.

45. Lin, R. Q.; Bak, S. M.; Shin, Y.; Zhang, R.; Wang, C. Y.; Kisslinger, K.; Ge, M. Y.; Huang, X. J.; Shadike, Z.; Pattammattel, A.; Yan, H. F.; Chu, Y.; Wu, J. P.; Yang, W. L.; Whittingham, M. S.; Xin, H. L.; Yang, X. Q. Hierarchical Nickel Valence Gradient Stabilizes High-nickel Content Layered Cathode Materials. *Nat. Commun.* **2021,** *12*, 1-10. DOI 10.1038/s41467-021-22635-w.

46. Zhang, K.; Li, B.; Zuo, Y.; Song, J.; Shang, H.; Ning, F.; Xia, D. Voltage Decay in Layered Li-rich Mn-based Cathode Materials. *Electrochem. Energy Rev.* **2019,** *2*, 606-623. DOI 10.1007/s41918-019-00049-z.

47. Li, T. Y.; Yuan, X. Z.; Zhang, L.; Song, D. T.; Shi, K. Y.; Bock, C. Degradation Mechanisms and Mitigation Strategies of Nickel-Rich NMC-Based Lithium-Ion Batteries. *Electrochem. Energy Rev.* **2020,** *3*, 43-80. DOI 10.1007/s41918-019-00053-3.

48. Liu, W.; Li, X. F.; Xiong, D. B.; Hao, Y. C.; Li, J. W.; Kou, H. R.; Yan, B.; Li, D. J.; Lu, S. G.; Koo, A.; Adair, K.; Sun, X. L. Significantly Improving Cycling Performance of Cathodes in Lithium Ion Batteries: The Effect of Al_2O_3 and $LiAlO_2$ Coatings on $LiNi_{0.6}Co_{0.2}Mn_{0.2}O_2$. *Nano Energy* **2018,** *44*, 111-120. DOI 10.1016/j.nanoen.2017.11.010.

For Table of Contents Use Only